Available online at www.CivileJournal.org

Civil Engineering Journal

(E-ISSN: 2476-3055; ISSN: 2676-6957)

Vol. 12, No. 03, March, 2026

Experimental Study of Cold-Formed Steel Bridge Girder in Various Shapes Under Static Loads

Ali Allami [1*], Haleem K. Hussain [2], Fareed H. Majeed [2]

[1] *Department of Civil Technologies, Technical Institute of Amara, Southern Technical University, Iraq.*

[2] *Department of Civil Engineering, Faculty of Engineering, University of Basrah, Basrah 61004, Iraq.*

Received 03 January 2026; Revised 19 February 2026; Accepted 22 February 2026; Published 01 March 2026

Abstract

To facilitate accelerated bridge construction and reduce the cost of bridge design and construction, a cold-formed steel composite bridge girder has been suggested recently as an economical alternative. The new technology for the composite bridge girder includes a cold-formed steel plate and either a precast or cast-in-place reinforced concrete (RC) slab. Previous research on cold-formed steel concrete composite girders has introduced two new shapes for short-span bridge girders: a cold-formed steel tub girder and a folded plate girder system. No study has been conducted on the impact of shape on the static structural behavior of cold-formed composite girders for short-span bridges. This paper investigated the behavior of the cold-formed steel composite girders with different shapes in terms of ductility, stiffness, the ultimate failure load, crack resistance, and interfacial slip. Four shapes were carried out in this research: tub, open-box, and double C with and without lips. Six simply supported girder specimens were designed, fabricated, and subjected to static load tests. The results showed that the cold-formed steel double C lipped girder increased the ultimate load by 12.12% compared to the cold-formed steel tub girder. Additionally, the initial stiffness of the cold-formed steel double C girder increased by 21% compared to the cold-formed steel tub girder. The open-box shape specimen can effectively improve the cracking resistance of cold-formed steel composite girders compared to the cold-formed steel tub girders.

Keywords: Cold-Formed Steel Composite Girder; Static Behavior; Experimental Study; Shapes of Cold-Formed Steel; Ultimate Failure Load.

1. Introduction

A composite girder of cold-formed steel plate and RC deck system has recently been proposed as an efficient option for accelerating bridge construction and reducing bridge design and construction costs [1-5]. The cold-formed steel composite girder is transported to the bridge location after complete prefabrication. Prefabrication is a widespread technique in bridge engineering based on prefabricating and assembling some bridge components on-site, reducing the need for cutting and welding plates. The total cost of folded-plate bridge girders was 20% less than the engineer's estimate, and the construction time was 33% less than that of a similar conventional bridge [1]. The cross-sectional geometries of cold-formed steel plates and the arrangement of shear connections greatly influence the performance of bridge girders under static and fatigue loads. The composite bridge girder consists of a cold-formed steel section and a precast or cast-in-place reinforced concrete deck slab connected to the steel section by shear connectors. The steel section girder is being manufactured with a high-capacity press-brake machine. Plates are positioned in the press-brake and cold-bent to achieve the specified bend radius. Another method of cold-formed composite girder construction is prefabrication [5, 6].

* Corresponding author: ali.allami@stu.edu.iq

https://doi.org/10.28991/CEJ-2026-012-03-021

The design of the cold-formed plate girder system started from 1978, when Kennedy et al. [7] designed a full-scale composite bridge girder of cold-formed steel and an RC deck slab. The steel box sections were fabricated by brake-forming half sections of steel sheet and welding them together to form boxes with the special V-shaped shear connectors (lugs). Taly & GangaRao [8] suggested a new T-Box bridge girder system using a composite tub girder from a steel plate bent by a press brake. An alternative method of concrete-steel composite girders was employed with WT steel sections welded to the steel plate deck to improve the longitudinal stiffness of the orthotropic deck. Nakamura [9] proposed a new composite bridge girder made of cold-formed steel. The girder consists of a U-shaped steel plate and two types of concrete: prestressed concrete at the middle span and conventional concrete at the end span. Burgueño & Pavlich [10] focused on verifying the concept of placing and post-tensioning prefabricated units (a press-brake box girder and slab) to achieve accelerated bridge construction. Adler et al. [11] proposed the Folded Plate Girder (FSPG) System (see Figure 1(a)). The Folded Steel Plate Girder (FSPG) System consists of inverted tub sections made by cold-bending flat plates using a brake-press machine with deck slabs precast or cast-in-place.

Other researchers advanced the system by conducting constructability testing on folded plate girders [12], the performance of the composite folded plate girder system under the action of fatigue loading [13], and performing analytical studies on the first folded plate girder bridge [1]. Recently, Kelly [14] studied the behavior of non-composite press-brake-formed steel tub girders. The experimental test was carried out on two non-composite girders. Barth et al. [15] developed the shallow press-brake-formed steel tub girders (PBFTG) of short-span bridges. The girder proposed by Michaelson is a composite of a steel tub section formed by press-brake and a reinforced concrete deck (RC) cast in place, connected to the tub steel girder by shear studs, as shown in Figure 1(b). Many researchers have studied press-brake-formed steel tub girders (PBFTG) to assess how well uncoated and galvanized girders perform over time [3], to evaluate girders with UHPC joints [16], and to expand the span length [17]. Tumbeva et al. [18] developed a new method to produce cold-formed tub composite girders. A web was cold-formed and bolted to top flanges and flat bottom plates in a built-up steel tub girder system. To improve the application of the press-brake-formed steel tub girder system, Morgan et al. [19] investigated the flexural behavior of press-brake-formed steel tub girders under low-skew angles. Previous Studies [5, 20-22] investigated the live load distribution factors for Press-Brake-Formed Tub Girder Bridges in the field and analytically.

Two new shape girder designs for short-span bridges have been developed from previous research on cold-formed steel concrete composite girders: the folded plate girder system and the cold-formed steel tub girder. No study has been conducted on the impact of shape on the static structural behavior of cold-formed composite girders for short-span bridges. To assess the behavior of the cold-formed composite bridge girder in terms of ductility, stiffness, ultimate failure load, crack resistance, and interfacial slip, four shapes of girder were designed, fabricated, and experimentally tested (see Figure 1(c)).

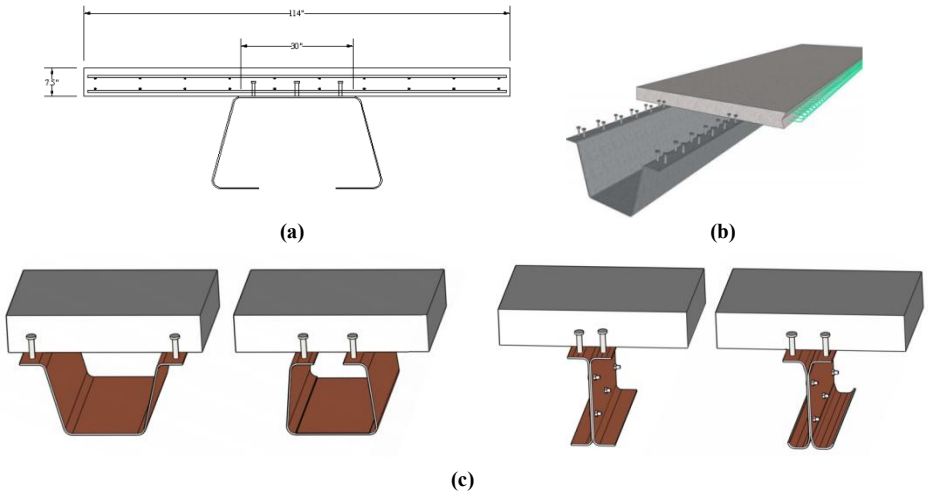

Figure 1. Cold-Formed Steel Composite Girder Proposed by (a) Michaelson (2014) [23], (b) Burner (2010) [13], (c) present study

2. Experimental Design

2.1. Specimen Design

Design of the composite girder was done by determining the properties of each shape chosen for the composite girder. Design iterations were completed based on conservative estimates of composite girder capacity [23]. Based on the design methodology conducted by Michaelson [23], the optimum depth of each shape was determined. Tub sections, open box sections, double C-sections, and double C-lipped sections were selected for practical application in steel bridges and cold-formed girder systems. The optimal depth of each shape is determined by the yield moments of specimens at various depths (see Table 1 and Figure 2). Figure 3 illustrates the flowchart of the experimental procedure, executed in two phases.

Table 1. Design comparison of Cold-Formed shapes composite girders

Specimen	My (kN-m)			
	d = 100 mm	d = 150 mm	d = 195 mm	d = 250 mm
Cold-Formed Tub Steel Composite Girder (CFT)	-	111.51	***112.72***	105.06
Cold-Formed Open-Box Steel Composite Girder (CFOB)	108.14	117.35	***119.51***	118.70
Cold-Formed Double C Steel Composite Girder (CFDC)	80.83	92.40	107.14	***113.95***
Cold-Formed Double C Lipped Steel Composite Girder (CFDCL)	80.70	92.74	106.89	***115.01***

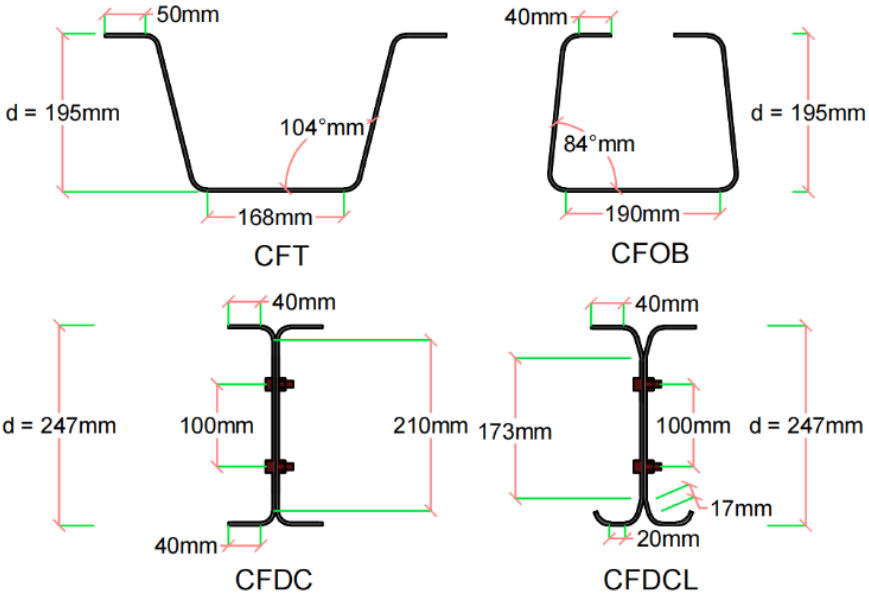

Figure 2. Cold-formed steel shapes of composite girders used in the present study

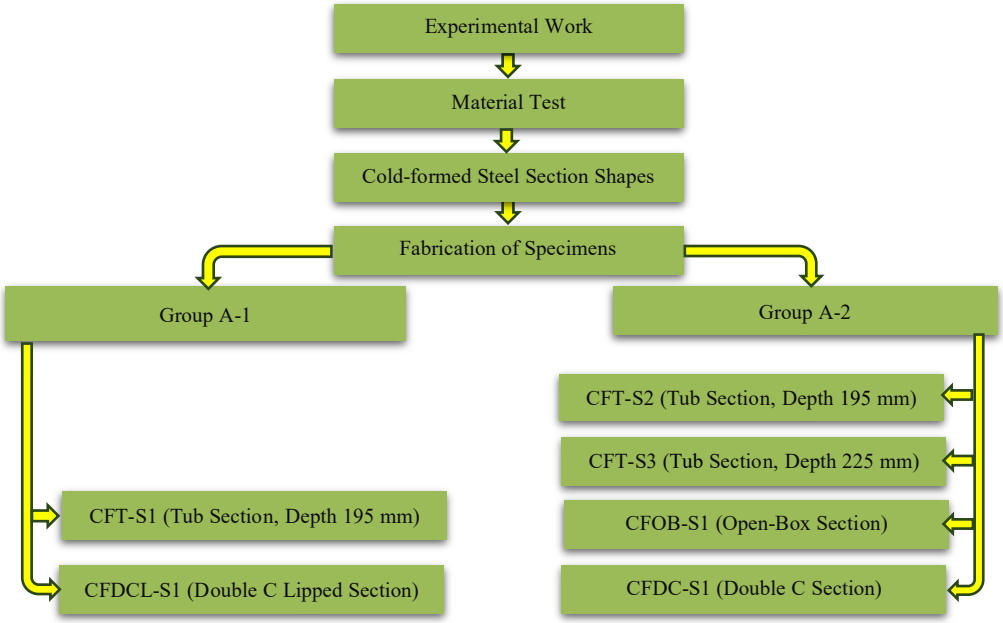

Figure 3. Flowchart of the experimental work

The experimental program was specifically designed as a comparative study to evaluate the effect of cross-sectional shape on structural behavior. The CFT steel section used in this study was chosen according to the scaling ratio of a steel section proposed by Michaelson [23]. CFT, CFOB, CFDC, and CFDCL specimens were designed to investigate the effect of shape on the behavior of composite girders under static tests. A CFT-S3 specimen was designed to investigate the depth effect of the cold-formed steel tub girder proposed by Michaelson [23]. All the specimens had a span length of 3 m, and the deck slab was 500 mm wide and 100 mm thick. Details of the cross-section specimens used in this paper are shown in Table 2 and Figure 4.

Table 2. Design comparison of Cold-Formed shapes composite girders

Specimen	d (mm)	Reinforcement pattern	Shape of Section
CFT-S1	195	A-1	Tub
CFDCL-S1	247	A-1	Double C Lipped
CFT-S2	195	A-2	Tub
CFT-S3	243	A-2	Tub
CFOB-S1	195	A-2	Open-Box
CFDC-S1	247	A-2	Double C

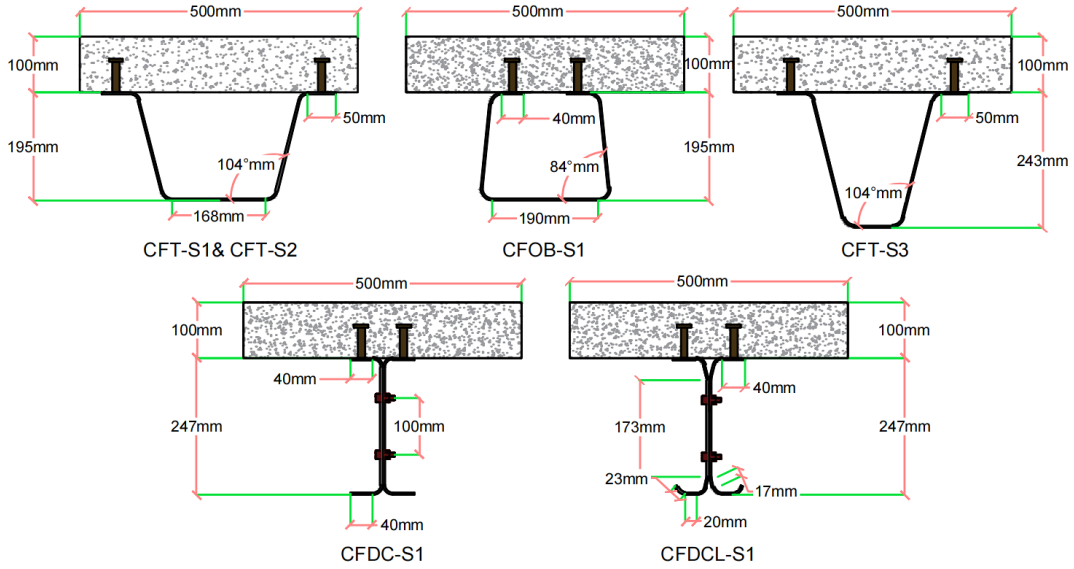

Figure 4. Shapes and dimensions of the cold-formed steel concrete girders (t = 3.7 mm)

Fabrication of the cold-formed steel girder specimen started with a single steel plate measuring 3000 mm × 700 mm × 3.70 mm for each specimen. Using the plate, four specimen shapes were formed using a high-capacity bending press brake, as shown in Figure 5(a). The plates were set in the press-brake machine and cold-bent to achieve the required bending radii. A stiffener plate was welded at the supports and point loads to prevent possible premature bearing failure during the flexural test (see Figure 5(b)). A shear stud single row of ϕ12.75 mm × 60 mm spacing at 150 mm was welded to each upper flange, designed as full interaction for all specimens, as illustrated in Figure 5(c). Following the completion of the steel girder manufacturing, wooden forms and reinforcement for the deck were erected around the specimens. The mixing truck was used for concrete pouring, and the specimens were left in place while the water curing continued for 28 days (see Figure 5(d)). Two patterns of reinforcement were designed for the specimens. First, the minimum area of steel reinforcement is used to understand the behavior of the cold-formed steel section, verify the fabrication process, and investigate the effect of reinforcement on specimen behavior. The second reinforcement pattern was designed based on the empirical deck method outlined in section 9.7.2 of the AASHTO LRFD specification (AASHTO 2010) [24], as shown in Figure 6. The double C-section was connected using a two-row 4.8mm bolt spacing of 200 mm (see Figure 7).

(a) **(b)**

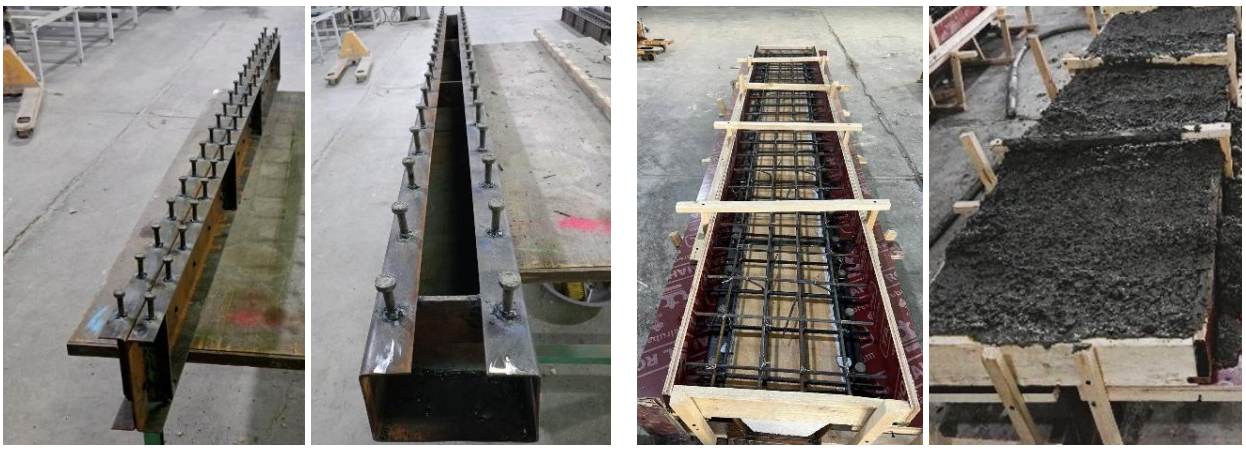

(c) (d)

Figure 5. Specimens' fabrication: (a) cold-formed plate, (b) welding the stiffeners plate, (c) welding the shear studs, (d) formwork, reinforcement and casting the specimens

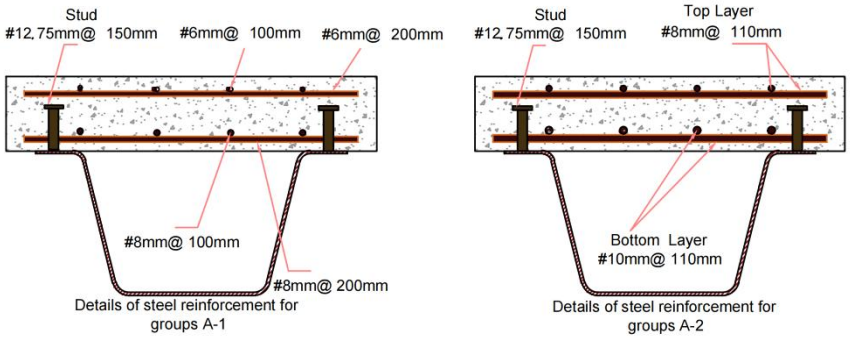

(a) (b)

Figure 6. (a) Deck reinforcement for specimens group A-1, (b) Deck reinforcement for specimens group A-2

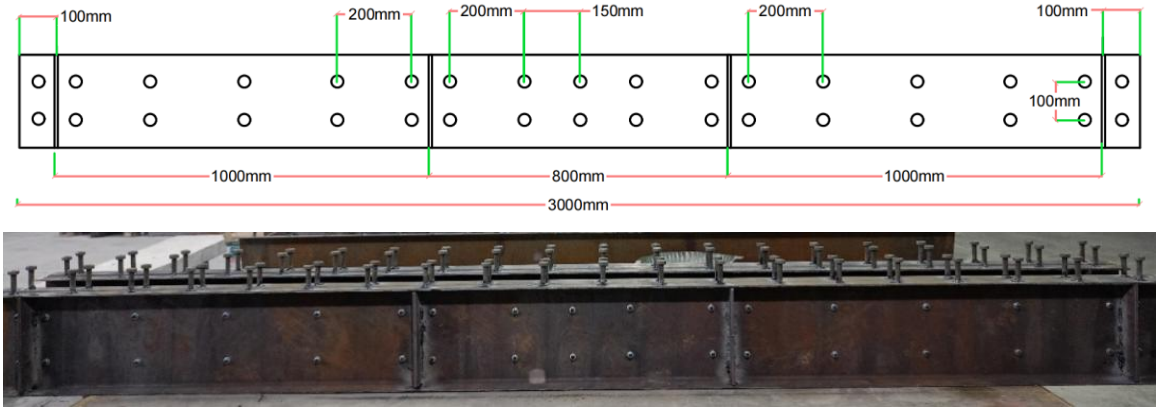

Figure 7. The connection of the specimens using bolts

2.2. Material Properties

The concrete mix is designed based on the ACI 211 specification [25], which depends on the properties of the materials. Several trial batches of the concrete mix design were cast to achieve the required compressive strength. The final mixing quantities were as indicated in Table 3. Three cubes of standard-weight concrete were cast for each specimen to be tested simultaneously, as outlined in references EN-BS 12390 [26] and British Standard [27]. The cubes were tested simultaneously with the specimens, and the average concrete compressive strength for all cubes was 36 MPa. Three samples of steel reinforcement for each diameter, with a length of 500 mm, were tested according to ASTM A615/A615M-22 [28] in the Construction Laboratory in the Technical Institute of Amara. Table 4 shows the properties of the samples tested for each of the steel plates [29], rebar reinforcement, and shear stud.

Table 3. Contents of the concrete mix

Cement (kg/m^3)	Fine aggregate (kg/m^3)	Coarse aggregate (kg/m^3)	Water (kg/m^3)	W/C ratio
430	725	930	194	0.45

Table 4. Shows the average properties of the samples tested

Sample	Yield strength (MPa)	Tensile strength (MPa)	Elongation (%)
Rebar 8 mm	568	665	13
Rebar 10 mm	559	699	11
Stud 12.75 mm	350	432	24
Steel plate 3.7 mm	335	419	28

2.3. Loading Program and Experimental Set-up

The load was applied using an MTS 600-kN servo-hydraulic actuator. The dimensions and test configuration are shown in Figure 8. Testing begins by recording the initial readings of the load and strain gauges, and then the load is applied in successive stages. At each stage, the readings of the load and strain gauges are recorded by a data logger, the appearance of cracks is noted, and marks are placed to identify their locations.

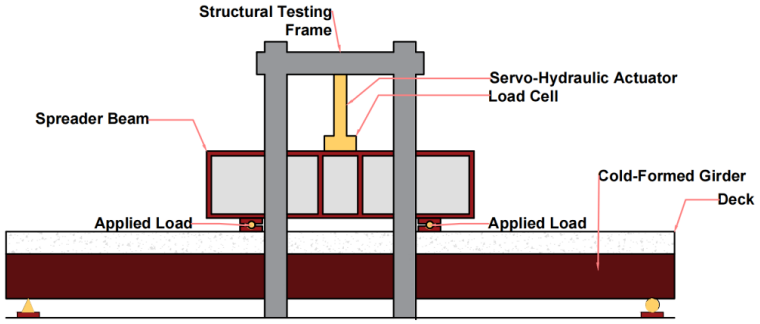

(a)

(b)

Figure 8. (a) Typical test setup layout, (b) Isometric view of a standard test setup

Vertical deflections were determined utilizing linear variable displacement transducers (LVDTs), each with a total range of 100 mm. Strain gages were used to measure at four levels across the girder's mid-span depth, as shown in Figure 9. Measurements were done using TML strain gauges and a GEODATALOG 8 data logger. These included one strain gauge mounted on the concrete surface top and three were installed along the bottom steel flange, top steel flange and web of the girder.

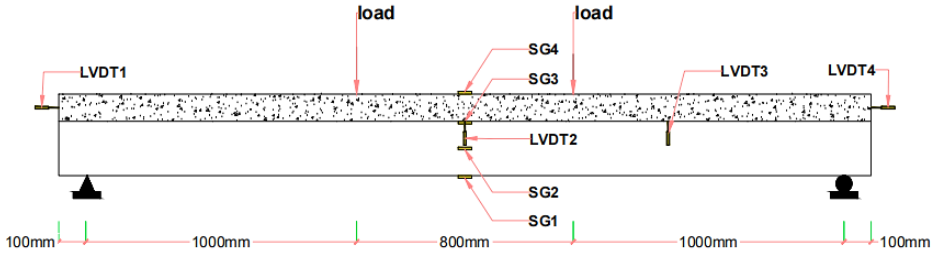

Figure 9. Shows a strain gauge location at four levels across the section depth of the specimen

3. Experimental Results and Discussion

3.1. Failure Modes of Group A-1

The specimens were simply supported under a four-point load and subjected to the same testing conditions. The load was applied gradually to the failure stage. The specimens failed similarly, with the concrete crushing the upper deck slab at mid-span. The main differences in failure modes among specimens were the first-crack load, ductility, stiffness, slip at the steel–concrete interface, and ultimate failure load.

The first crack appears at 190 kN and flexural cracks propagate at mid-span with increased applied load for the CFT-S1 specimen, and another shear-flexural crack appears outside the load point because the longitudinal edge of the deck slab is subjected to concentrated shear stress according to the shape configuration of tub section and the location of the shear studs, as shown in Figure 10(a). The yield load of the CFT-S1 specimen was 210 kN before reaching the 264 kN failure load. After failure, crushing concrete at the top deck slab and local buckling were observed in the top steel flange of CFT-S1specimen, similar to the failure mode achieved by Woldegabriel [20] (see Figure 10(b)).

CFDCL-S1 Specimen represents the cold-formed double C steel section with a lip bottom flange for the section and the same dimensions of deck slab as the CFT-S1 specimen. The failure mode of the CFDCL-S1 specimens was crushing concrete at the top deck slab without the appearance of a shear-flexural crack or buckling in the steel plate section, as shown in Figure 10(b). The first crack, yield, and ultimate loads of the CFDCL-S1 specimen were higher than those of the CFT-S1 specimen, at 215 kN, 220 kN, and 296 kN, respectively.

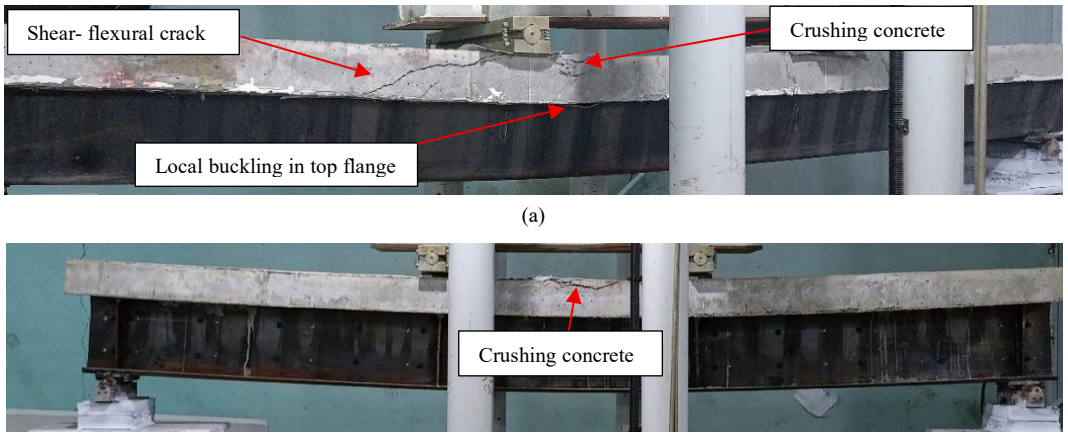

Figure 10. (a) Failure modes of CFT-S1 specimen, (b) Failure modes of CFDCL-S1 specimen.

3.2. Failure Modes of Group A-2

Table 6 shows the results of the load and failure mode tests. The CFT-S2 specimen has the same dimensions and properties as the CFT-S1 specimen. The steel reinforcement of the deck for the CFT-S2 specimen is designed according to section 9.7.2 of the AASHTO LRFD specification. The first crack appeared in the CFT-S2 specimen at a load of 200 kN. As the applied load increased, more cracks propagated at the mid-span of the girder, and a shear-flexural crack appeared in a width less than that of the CFT-S1 specimen, which was achieved by increasing the reinforcement in the deck slab. The yield and ultimate load of the CFT-S2 specimen were 211 kN and 281 kN, respectively. The failure mode was observed as crushing the top concrete deck slab at the mid-span of the girder without local buckling in the top steel flange section, as in the CFT-S1 specimen (see Figure 11(a)). The failure mode of the CFT-S3 specimen was similar to that of the CFT-S1 and CFT-S2 specimens, but the first crack occurred at 240 kN. Additionally, the shear-flexural and flexural crack widths were less. The yield and ultimate loads of the CFT-S3 specimen were higher compared to the CFT-S2 specimen, equal to 222 kN and 302 kN, respectively. A crush of concrete was observed at mid-span on the top deck slab girder when reaching the failure load, as shown in Figure 11(b). The first crack appeared in the CFOB-S1 specimen at 230 kN, and the ultimate failure load was 284 kN. Figure 11(c) illustrates that the final failure mode of the CFOB-S1 specimen involved crushing concrete at the top of the deck without a shear-flexural crack appearing. Specimen CFDC-S1 represents the cold-formed steel double C section and the same properties of the deck slab for the CFT-S2 specimen. The failure mode of the CFDC-S1 specimen is similar to the CFT-S2 specimen, without noting a shear-flexural crack. The first crack was at a load of 225 kN, culminating in an ultimate failure load of 305 kN, accompanied by concrete crushing at the top deck slab (see Figure 11(d)).

Experimental results show that using steel reinforcement for the deck slab per AASHTO improved ductility, increasing the ultimate load by 6.44% (see Table 6) and reducing the length and width of the shear-flexural crack. Increasing the depth of the cold-formed steel tub section from 195 mm to 243 mm increased the ultimate load by 15.53% and resulted in a reduction in both the length and width of the shear-flexural crack. Furthermore, results from the CFT-

S1 and CFDCL-S1 specimen tests indicated that a 12.12% increase in the ultimate load was achieved by using the double C-lipped specimen. Additionally, the ultimate load of the double C specimen (CFDCL-S1) is higher than that of the tub section (CFT-S2) by 8.54%.

Table 6. Results of the static test

Group	Specimen	First crack load kN	Yield load kN	Ultimate load kN	Crack	Failure mode
A-1	CFT-S1	190	210	264	Shear-flexural crack and flexural crack	Crushing of concrete at the compression zone and local buckling in the top flange.
	CFDCL-S1	215	220	296	Flexural crack	Crushing of concrete at the compression zone.
A-2	CFT-S2	200	211	281	Shear-flexural crack and flexural crack	Crushing of concrete at the compression zone
	CFT-S3	240	222	302	Shear-flexural crack and flexural crack	Crushing of concrete at the compression zone
	CFOB-S1	230	207	284	Flexural crack	Crushing of concrete at the compression zone
	CFDC-S1	225	236	305	Flexural crack	Crushing of concrete at the compression zone

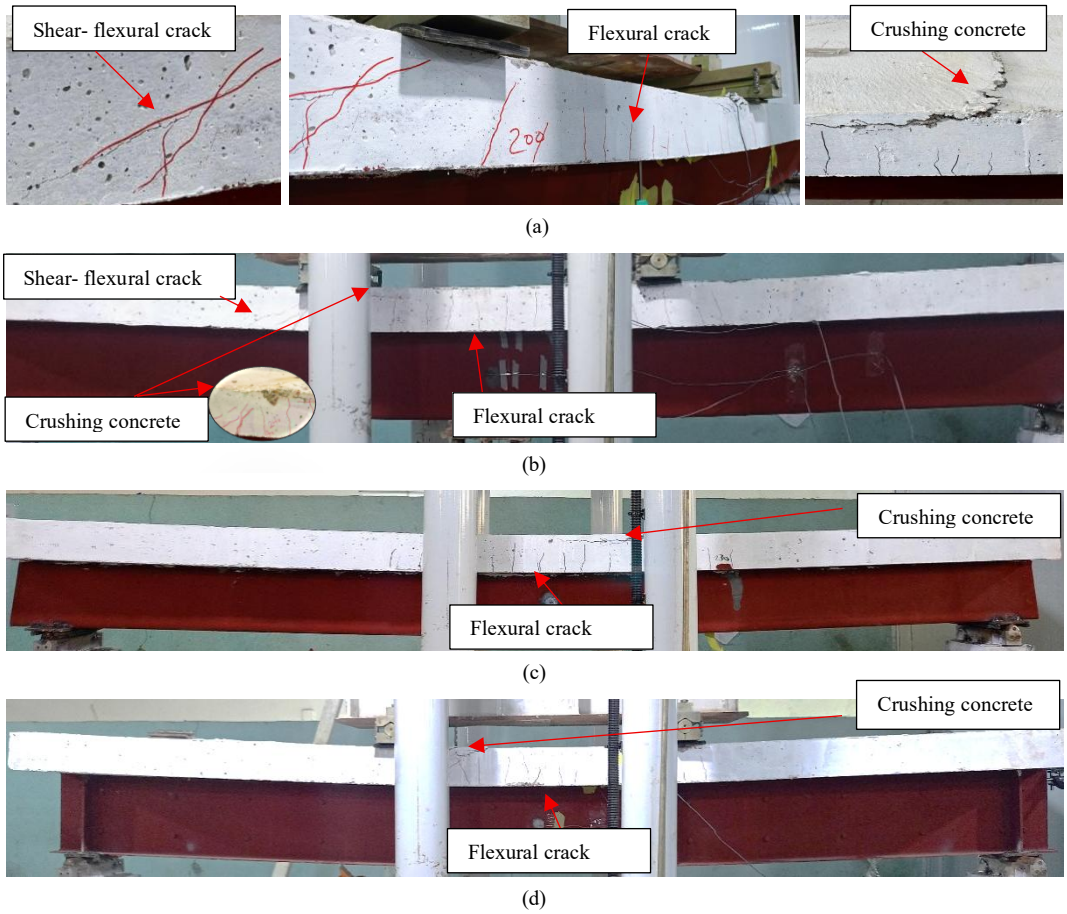

Figure 11. Failure modes: (a) CFT-S2 specimen, (b) CFT-S3 specimen, (c) CFOB-S1 specimen, (d) CFDC-S1 specimen

3.3. Load Defection Curve of Specimens

The load-deflection curve of the composite bridge girder allows for characterization of its behavior as either brittle or ductile. The stiffness is defined as the slope of the load-deflection relationship as described by the following equation:

$$\text{Stiffness (kN/mm)} = \frac{load}{defelction} \quad (1)$$

The stiffness of specimens is determined based on the load before reaching the first crack load at service load [30]. Figure 12 shows the load-deflection relationship for specimens, with deformations monitored using Linear Variable Deflection Transformers (LVDTs). The curves consist of two phases: an initial elastic phase, where deflection increases linearly with load, and an elastic-plastic phase, where deflection increases more rapidly. The load-deflection curve of the CFT-S1 specimen with minimum reinforcement for the deck slab indicates that failure occurred before it reached its ultimate capacity. In contrast, the CFT-S2 specimen reached its ultimate load, where the deck slab steel reinforcement ratio was increased as specified by AASHTO, Figure 13.

Comparing specimens with different cold-formed steel sections, the use of double C-sections increased the girder stiffness and reduced mid-span deflection under the same load. Table 7 shows the initial stiffness at the service load before the first crack load is reached. The initial stiffness of the cold-formed double-c steel section increased from 15.04 kN/mm to 18.15 kN/mm (a 21% increase compared to CFT-S2). The stiffness of the CFT-S3 specimen (tub section, 243 mm depth) was 16.24 kN/mm (8 % increase compared to CFT-S2). The stiffness of the remaining specimens is shown in Table 7.

Table 7. Stiffness of specimens at service load

	Group A-1		Group A-2			
Specimen	**CFT-S1**	**CFDCL-S1**	**CFT-S2**	**CFT-S3**	**CFDC-S1**	**CFOB-S1**
Deflection at yield point mm	15.20	15.80	16.00	16.00	14.50	14.00
Yield load kN	210.00	220.00	211.00	222.00	236.00	207.00
Deflection at service load mm	11.20	12.50	12.50	12.40	11.20	12.00
Service load kN	176.60	197.60	188.00	201.33	203.33	190.00
Stiffness	15.77	15.81	15.04	16.24	18.15	15.83

3.4. The Ductility

The ductility factor is calculated by dividing the deflection value at the yield load by the deflection value at the failure load, as described by the following equation [31]:

$$\text{Ductility factor} = \frac{deflection\ at\ yield\ load}{deflection\ at\ ultimate\ load} \quad (2)$$

Table 8 illustrates the ductility factor of specimens. The CFT-S1 specimen failed before reaching ultimate capacity, resulting in a 48% decrease in the ductility factor compared to the CFDCL-S1 specimen. Ductility improvement and failure occur at larger deflections when the deck's steel reinforcement is designed in accordance with AASHTO for a tub section specimen. The ductility factor of the CFOB-S1 specimen was a higher value compared to the other specimens of the static test, equal to 3.32.

The results showed that the ductility factor was relatively equal for the four different steel section shapes of specimens under static load. Furthermore, the CFDC-S1 specimen had the highest failure load and stiffness (Table 7).

Table 8. Ductility Factor of Specimen

	Group A-1		Group A-2			
Specimen	**CFT-S1**	**CFDCL-S1**	**CFT-S2**	**CFT-S3**	**CFDC-S1**	**CFOB-S1**
Deflection at yield point, *Δy* mm	15.20	15.80	16.00	16.00	14.50	14.00
Yield load kN	210.00	220.00	211.00	222.00	236.00	207.00
Deflection at ultimate load, Δu (mm)	31.70	49.00	52.83	52.00	47.35	46.48
ultimate load kN	264.90	296.40	281.00	302.00	305.00	285.00
Ductility Factor	2.09	3.10	3.30	3.25	3.27	3.32

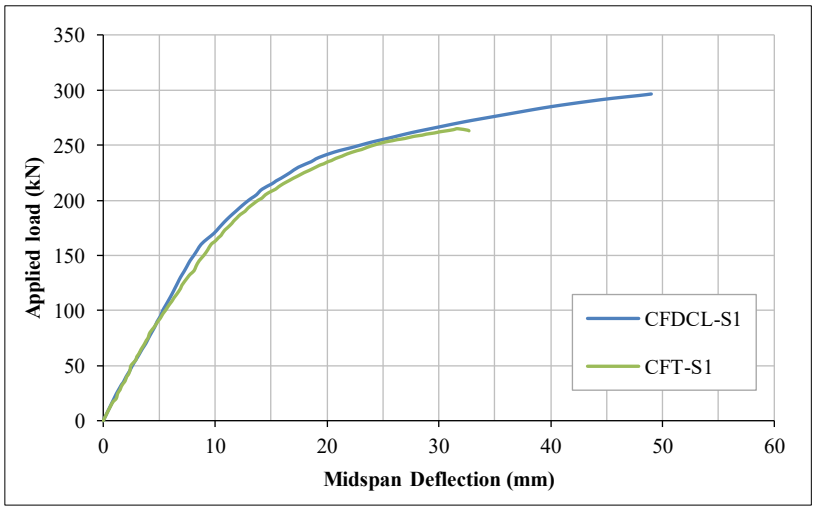

(a)

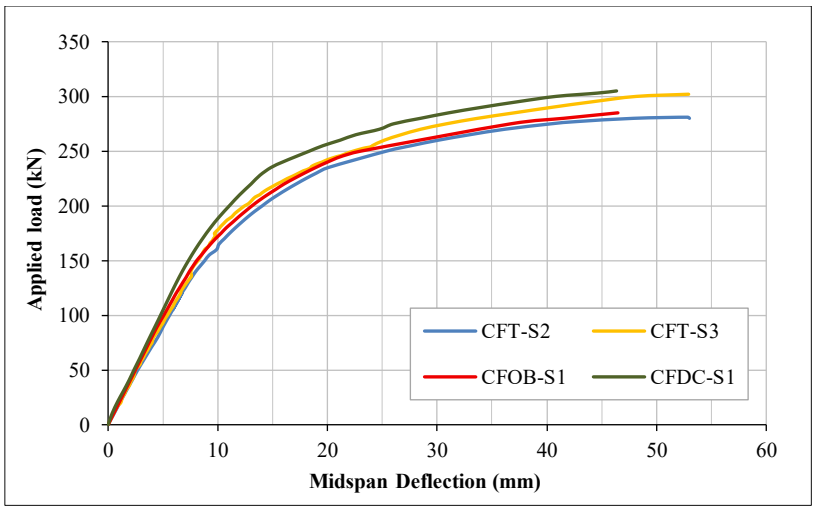

(b)

Figure 12. (a) load-deflection curve of group A-1 specimens, (b) load-deflection curve of group A-2 specimens

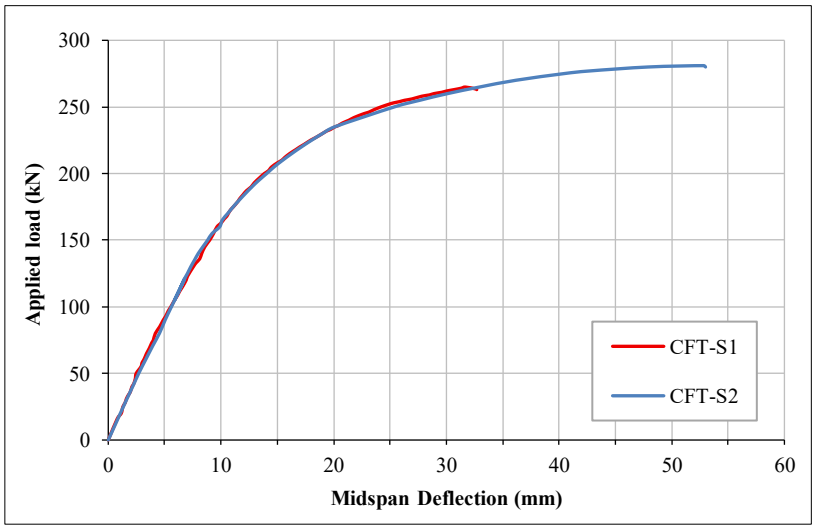

Figure 13. load-deflection of specimens with different ratios of steel reinforcement

3.5. Strain of Specimens

The strain of the concrete deck slab

The strain of the concrete deck slab was measured using strain gauges installed on its surface, denoted SG4. The load-strain curves for the concrete deck slab at the mid-span section are illustrated in Figure 14. A significant increase occurred in specimens after concrete cracking. The specimens achieve or approach the maximum strain in the concrete. Consequently, all specimens failed due to concrete crushing during the test.

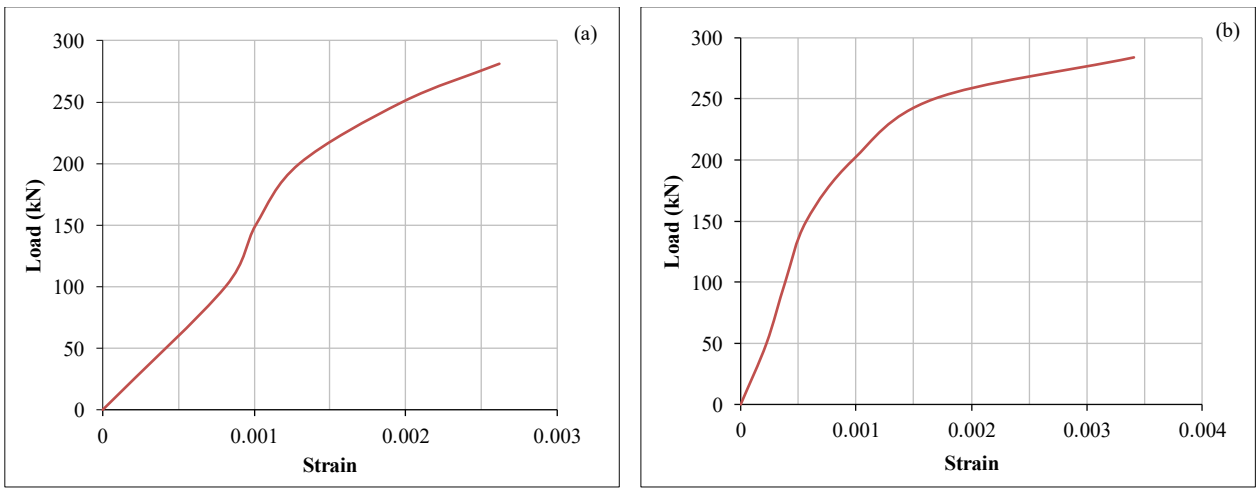

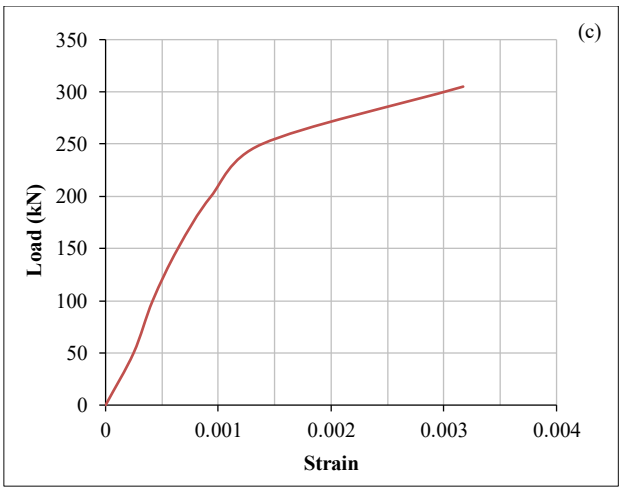

Figure 14. The strain of concrete (SG4), (a) CFT-S2 specimen (b) CFOB-S1specimen (c) CFDC-S1specimen

The cold-formed steel section strain

Steel section strain was recorded by strain gauges installed at the mid-span sections of the cold-formed steel section girder. Strain gauges SG1 and SG3 were placed at the top and bottom flanges of the steel girders, except for the SG3 CFOB-S1, which was plotted on the bottom surface of the concrete deck. Strain gauges SG2 were placed on the steel web of the cold-formed steel section girder. The strain results are shown in Figure 15. The increasing stiffness of the CFDC-S1 specimen results in higher yield stresses for the steel bottom flange compared to the CFT-S2 and CFOB-S1 specimens at the same load, as shown in Figure 16. Hence, the bottom-flange strain is affected by the shape of the cold-formed steel section.

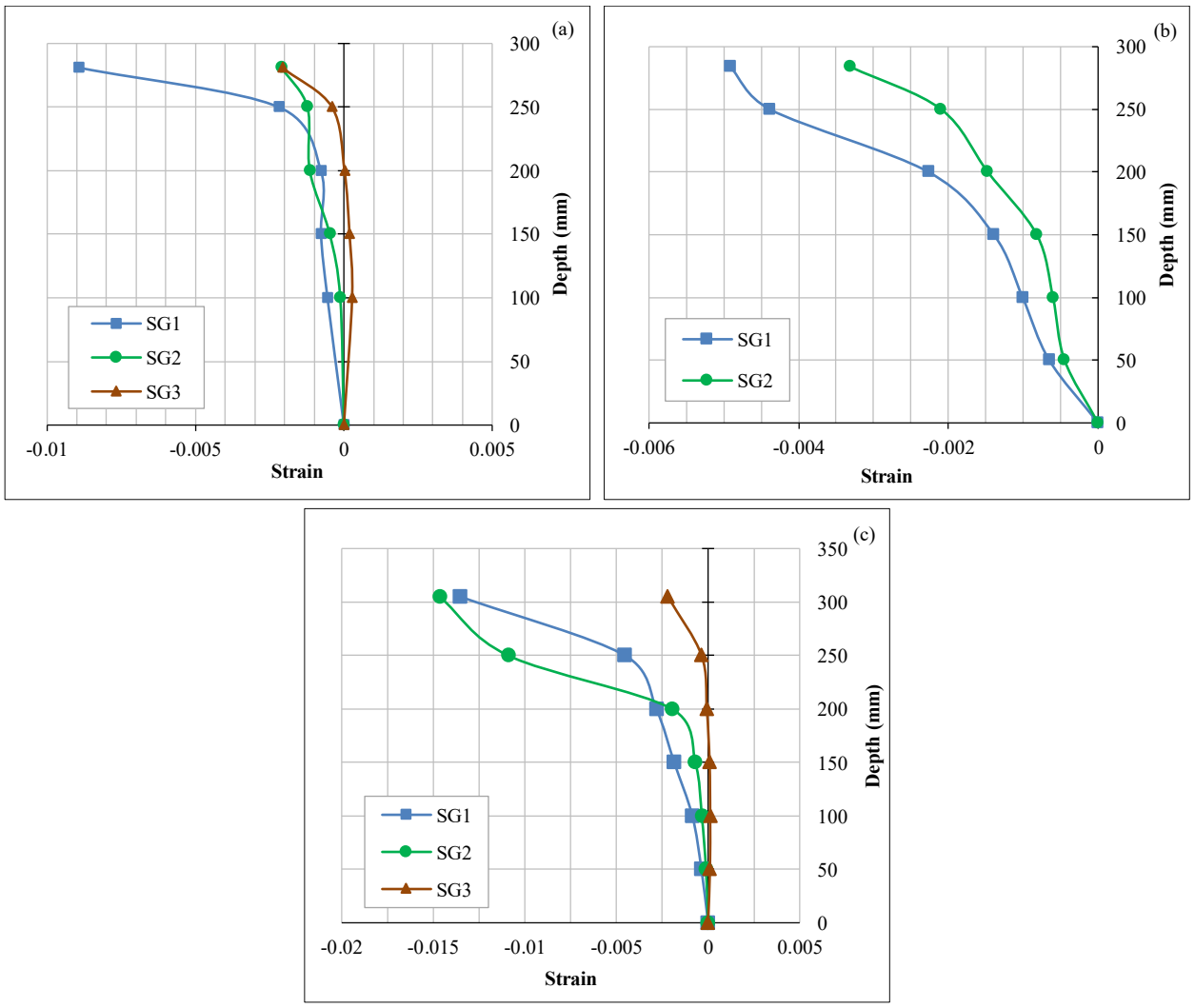

Figure 15. strain of cold-formed steel section (a) CFT-S2 specimen (b) CFOB-S1specimen (c) CFDC-S1specimen

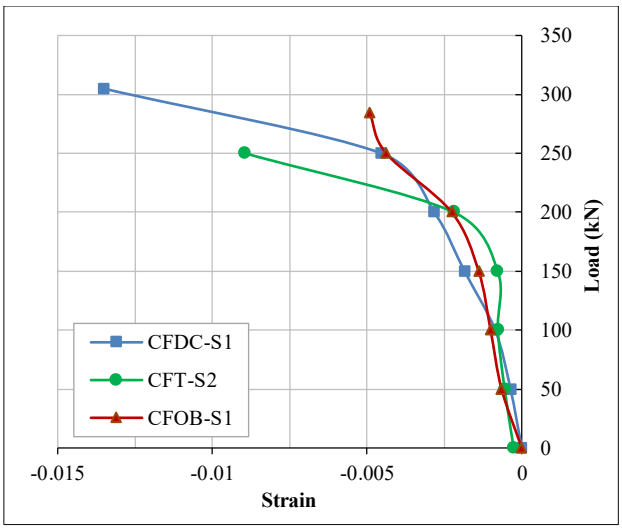

Figure 16. The load-strain curves for the cold-formed steel bottom flanges of the specimens

3.6. Slip at the Steel–Concrete Interface

The distributions of slip at the steel–concrete interface of the girder ends under various load levels for each specimen are illustrated in Figure 17. It can be observed that the cold-formed steel tub girder for specimens CFT-S1, CFT-S2, and CFT-S3 had higher slip compared to other shapes. Also, the slip in the CFT-S3 specimen was reduced to 100% when the girder depth was increased. The slip at the interface for the CFT-S2 and CFT-S3 specimens is 4.3 times and 2 times higher, respectively, compared to the CFDC-S1 specimen at the end of the test. In addition, no slip was observed in the CFDCL-S1 specimen until failure. The configuration of the cold-formed composite girder influences slips by changing the distance between the upper flanges. As the distance between shear connectors increases, the gap widens, leading to greater slip at the ends.

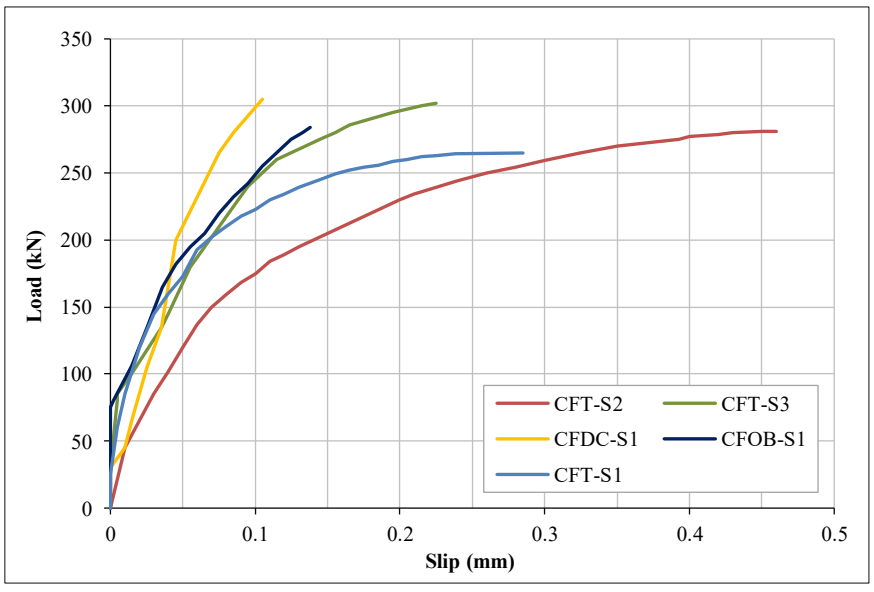

Figure 17. A slip of the steel–concrete interface at the end of the specimens under various load levels

4. Conclusions

The main objective of this study is to investigate the static behavior of cold-formed steel composite girders with various shapes under four-point static loads. Six simply supported girder specimens were designed, fabricated, and subjected to static load tests. The study examined the impact of different shapes of cold-formed steel sections on the performance of the composite bridge girder in terms of ductility, stiffness, ultimate failure load, crack resistance, and interfacial slip. Several conclusions can be listed as follows:

- The cold-formed steel double C lipped girder (CFDCL-S1) increased the ultimate load by 12.12% and has higher ductility compared to the cold-formed steel tub girder (CFT-S1).

- The initial stiffness of the cold-formed steel double C girder (CFDC-S1) increased by 21 % compared to the cold-formed steel tub girder (CFT-S٢).
- Increasing the depth of the cold-formed steel tub section for the CFT-S3 specimen from 195 mm to 243 mm increased the ultimate load by 15.53% externally while simultaneously decreasing the length and width of the shear-flexural crack.
- In case steel reinforcement of the deck slab is designed according to AASHTO for a tub section specimen, the ductility factor improvement and the specimen failure occur at a higher deflection.
- The CFOB-S1 (open-box shape) specimen can effectively improve the cracking resistance of cold-formed steel composite girders. Compared to the specimen CFT-S2, the cracking load of the specimen CFOB-S1 is 20% ratio higher.
- Shear-flexural cracks appeared only in the tub section specimens. Furthermore, the cold-formed steel tub girder collapsed early with minimal reinforcement of the deck slab, whereas the double C lipped section appeared more ductile.
- The cold-formed steel tub girders produced greater interfacial slip compared to the other shape specimens. In addition, no slips were noted in the CFDCL-S1 Specimen until failure.

In summary, compared to steel tub sections, cold-formed steel composite bridge girders with a double C steel section exhibit higher stiffness, a higher ultimate load capacity, improved crack resistance in static load tests, and lower interfacial slip. Additionally, the CFDCL-S1 specimen performs better in terms of ductility compared to the CFT-S1 specimen for group A-1. The cold-formed steel composite bridge girder with an open-box steel section, rather than tub steel section, exhibits almost no change in bending stiffness and ultimate load-bearing capacity. At the same time, there is a significant improvement in crack resistance under static load test, with a lower interfacial slip than using a steel tub section.

5. Declarations

5.1. Author Contributions

Conceptualization, A.A.; methodology, A.A.; software, A.A.; validation, A.A., H.K.H., and F.H.M.; formal analysis, A.A.; writing—original draft preparation, A.A.; writing—review and editing, A.A.; supervision, H.K.H. and F.H.M.; project administration, H.K.H. and F.H.M. All authors have read and agreed to the published version of the manuscript.

5.2. Data Availability Statement

The data presented in this study are available in the article.

5.3. Funding

This work was partially supported by Southern Technical University and Basrah University under scientific research awards, No. 9/7934, 10 Sep. 2025.

5.4. Conflicts of Interest

The authors declare no conflict of interest.

6. References

[1] Civjan, S. A., Sit, M. H., & Breña, S. F. (2016). Field and Analytical Studies of the First Folded-Plate Girder Bridge. Journal of Bridge Engineering, 21(11). doi:10.1061/(asce)be.1943-5592.0000918.

[2] Barth, K. E., Michaelson, G. K., & Tennant, R. M. (2020). Fatigue performance of singular and modular press-brake-formed steel tub girders. Bridge Structures, 16(1), 3–13. doi:10.3233/BRS-200168.

[3] Tennant, R. M. (2018). Fatigue performance of uncoated and galvanized composite press-brake-formed tub girders (Master's Thesis). West Virginia University, Virginia, United States.

[4] Deng, Y., Phares, B. M., & Steffens, O. W. (2016). Experimental and numerical evaluation of a folded plate girder system for short-span bridges - A case study. Engineering Structures, 113, 26–40. doi:10.1016/j.engstruct.2016.01.027.

[5] Barth, K. E., Michaelson, G. K., Roh, A. D., & Tennant, R. M. (2021). Field Determined Live Load Distribution Factors for Modular Press-Brake-Formed Tub Girders. Transportation Research Record, 2675(3), 1–7. doi:10.1177/0361198120983757.

[6] Gibbs, C. L. (2017). Field performance assessment of press-brake-formed steel tub girder superstructures (Master's Thesis). West Virginia University Libraries, Virginia, United States.

[7] Kennedy, J. B., Madugula, M. K. S., Keen, R. G., & Fung, C. (1978). Cold-Formed Steel in Composite Bridge Construction. Canadian Journal of Civil Engineering, 5(2), 164–173. doi:10.1139/l78-021.

[8] Taly, N., & Gangarao, H. V. S. (1979). Prefabricated Press-Formed Steel T-Box Girder Bridge System. Engineering Journal, 16(3), 75–83. doi:10.62913/engj.v16i3.337.

[9] Nakamura, S. (2002). Bending Behavior of Composite Girders with Cold Formed Steel U Section. Journal of Structural Engineering, 128(9), 1169–1176. doi:10.1061/(asce)0733-9445(2002)128:9(1169).

[10] Burgueño, R., & Pavlich, B. S. (2008). Evaluation of prefabricated composite steel box girder systems for rapid bridge construction (Research Report RC-1507). Department of Civil and Environmental Engineering, Michigan State University, Michigan, United States.

[11] Adler, S. (2017). A new era at Eastman. In Building bridges with music: Stories from a composer's life. Boydell & Brewer, 137–142. doi:10.1017/9781576472682.015.

[12] Glaser, L. A. (2010). Constructability testing of folded plate girders. University of Nebraska–Lincoln, Lincoln, United States.

[13] Burner, K. A. (2010). Experimental Investigation of Folded Plate Girders and Slab Joints Used in Modular Construction. Civil Engineering Theses, Dissertations, and Student Research, University of Nebraska, Lincoln, United States.

[14] Kelly, L. T. (2014). Experimental evaluation of non-composite shallow press-brake-formed steel tub girders. West Virginia University Libraries, Virginia, United States. doi:10.33915/etd.5958.

[15] Barth, K. E., Michaelson, G. K., & Barker, M. G. (2015). Development and Experimental Validation of Composite Press Brake–Formed Modular Steel Tub Girders for Short-Span Bridges. Journal of Bridge Engineering, 20(11), 04015007. doi:10.1061/(asce)be.1943-5592.0000770.

[16] Kozhokin, P. (2016). Evaluation of modular press-brake-formed tub girders With UHPC joints. West Virginia University, Virginia, United States. doi:10.33915/etd.6010.

[17] Tennant, R. M. (2022). Expanding the applicability of press-brake-formed tub girders through the extension of the maximum span length and the evaluation of pier continuity (Doctoral dissertation). West Virginia University, Virginia, United States. doi:10.33915/etd.11405.

[18] Tumbeva, M. D., Mutoka, S. C., Thrall, A. P., Zoli, T. P., Wagner, S., & Baah, P. (2023). Built-Up Press Brake-Formed Tub Girders. Journal of Bridge Engineering, 28(12), 4023092. doi:10.1061/jbenf2.beeng-6103.

[19] Morgan, M. L. (2024). The impact of low-skew on the ultimate capacity of press-brake-formed tub girders (Master's thesis). West Virginia University, Virginia, United States. doi:10.33915/etd.12456.

[20] Woldegabriel, B. T. (2023). Development and validation of improved live load distribution factors for moment in press-brake-formed steel tub girder bridges (Master's thesis). West Virginia University, Virginia, United States. doi:10.33915/etd.12197.

[21] Barth, K. E., Michaelson, G. K., Pyrialakou, V. D., Woldegabriel, B. T., Mason, J. R., & Tennant, R. M. (2025). Enhancing Live Load Distribution Predictions for Press-Brake-Formed Tub Girder Bridges for Moments in Interior Girders: A Statistical Approach. Journal of Bridge Engineering, 30(6). doi:10.1061/jbenf2.beeng-6440.

[22] Barth, K. E., Michaelson, G. K., Pyrialakou, V. D., Woldegabriel, B. T., & Tennant, R. M. (2025). Applicability and validation of improved live load distribution factors for commercially available shallow steel tub girders. Bridge Structures, 21(2–3), 81–92. doi:10.1177/15732487251330406.

[23] Michaelson, G. K. (2014). Development and feasibility assessment of shallow press-brake-formed steel tub girders for short-span bridge applications (Doctoral dissertation). West Virginia University, Virginia, United States. doi:10.33915/etd.6227.

[24] AASHTO. (2010). AASHTO LRFD bridge design specifications. American Association of State Highway and Transportation Officials, Washington D.C., United States.

[25] ACI Committee 211. (1974). Proposed revision of ACI 211-65: Recommended practice for selecting proportions for no-slump concrete. ACI Journal Proceedings, 71(4), 153–170. doi:10.14359/11176.

[26] BS EN 12390-1. (2001). Testing hardened concrete – Part 1: Shape, dimensions and other requirements for specimens and moulds. British Standards Institution (BSI), London, United States.

[27] BS EN (2009):12390-3. (2009). Testing hardened concrete." Compressive strength of test specimens. British Standards Institution (BSI), London, United States.

[28] ASTM A615/A615M-22. (2022).: Standard specification for deformed and plain carbon-steel bars for concrete reinforcement. ASTM International, Pennsylvania, United States.

[29] ASTM A370-17. (2017). Standard test methods and definitions for mechanical testing of steel products. ASTM International, Pennsylvania, United States.

[30] Nariman, N. A., Hamdia, K., Ramadan, A. M., & Sadaghian, H. (2021). Optimum design of flexural strength and stiffness for reinforced concrete beams using machine learning. Applied Sciences, 11(18), 8762. doi:10.3390/app11188762.

[31] Huang, Q., Liu, Y., Guo, Z., & Ju, J. W. W. (2025). Flexural fatigue strength of RC bridge girders strengthened by PHSW-PM. Engineering Structures, 338, 120640. doi:10.1016/j.engstruct.2025.120640.